Supporting information

Realizing high thermoelectric performance in Ag-doped PbSe by morphology engineering

Yu Tian [a], Li Ma [a, b], Zhifang Zhou [c], Guang-Kun Ren [a,], Yuansen Li [b], Zhijie Wei [a], Yan Shi [a], Yiying Zhao [a], Yuan-Hua Lin [c]*

[a] *Institute of Materials, China Academy of Engineering Physics, Jiangyou, Sichuan, 621908, P. R. China*

[b] *School of Physics, University of Electronic Science and Technology of China, Chengdu, Sichuan, 611731, China*

[c] *State Key Laboratory of New Ceramics and Fine Processing, Department of Materials Science and Engineering, Tsinghua University, Beijing, 100084, P. R. China*

Section 1: Related thermal properties

The thermal diffusivity (*D*) was measured by laser flash method (LFA-457, Netzsch, Germany) under a continuous Argon flow and the data is shown in Fig. S1a.

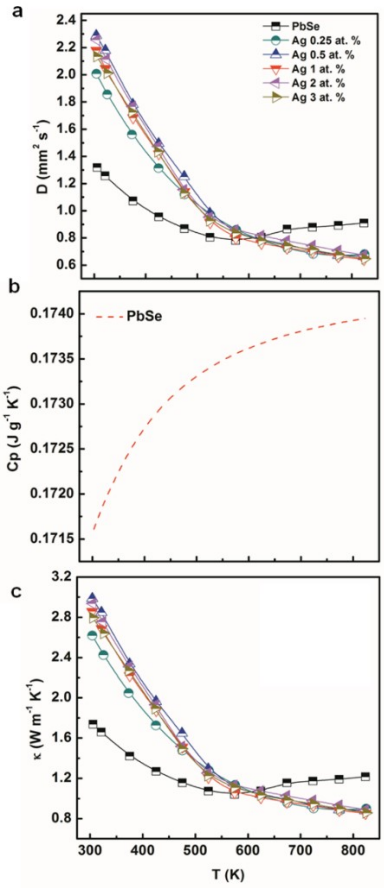

Supporting information

Fig. S1 (a) The measured thermal diffusion coefficient and (b) the specific thermal capacity as calculated by Debye model.

The specific heat capacity C_p is supposed to be very similar to C_v in bulk materials, and C_v can be deduced from the Debye model. As the thermal capacity would not change a significant amount with a small nominal Ag content (0-3 at. %), we calculated the C_p of pure PbSe and applied it for all samples, as shown in Fig. S1b, which was reasonable and the uncertainty could be neglected. The empirical formula is as follows:

$$C_V = \frac{3k_B V}{2\pi^2 v^3}\left(\frac{k_B T}{\hbar}\right)^3 \int_0^{\frac{\Theta_D}{T}} \frac{x^4 e^x}{(e^x-1)^2}\,dx, \tag{1}$$

where $x = \hbar\omega / k_B T$ is a dimensionless quantity, $\hbar$ Planck's constant, k_B the Boltzmann constant, ω is the phonon frequency, Θ_D is the Debye temperature (~191K).[1] The total thermal conductivity of all samples are calculated based on $\kappa = DC_p\rho$ and shown in Fig. S1c.

Section 2: Lorenz number and effective mass

In order to analyze the transport properties of samples, we measured their carrier concentration and mobility by Hall effect system, and based on single band model and electron-phonon interaction, the Lorenz number (see graph Fig. S2a) and the effective mass can be expressed as follows (the effective mass depends on the reduced Fermi energy η decreases with increasing temperature):

$$S = \pm\frac{k_B}{e}\left(\frac{(r+5/2)F_{r+3/2}(\eta)}{(r+3/2)F_{r+1/2}(\eta)} - \eta\right) \tag{2}$$

$$n = \frac{1}{2\pi^2}\left(\frac{2m^* k_B T}{\hbar^2}\right)^{3/2} F_{1/2}(\eta) \tag{3}$$

$$F_i(\xi) = \int_0^\infty \frac{x^i dx}{1+e^{x-\xi}} \tag{4}$$

$$L = \left(\frac{k_B}{e}\right)^2\left(\frac{(r+7/2)F_{r+5/2}(\eta)}{(r+3/2)F_{r+3/2}(\eta)} - \left[\frac{(r+5/2)F_{r+3/2}(\eta)}{(r+3/2)F_{r+1/2}(\eta)}\right]^2\right) \tag{5}$$

where e is the electronic charge, F_i is the Fermi integrals, and $\eta = E_F / k_B T$ is the reduce Fermi level, E_F is the electron Fermi level measured upward from the band edge. Meanwhile, acoustic phonon scattering ($r = -1/2$) has been assumed as the main carrier scattering mechanism. The effective mass is calculated by Equation (2-4). The Lorenz number can be obtained by applying the calculated reduced Fermi energy η and scattering parameter r into Equation (5).[2] κ_e is calculated and shown in Fig. S2b according to the Wiedemann–Franz law, $\kappa_e = L\sigma T$.

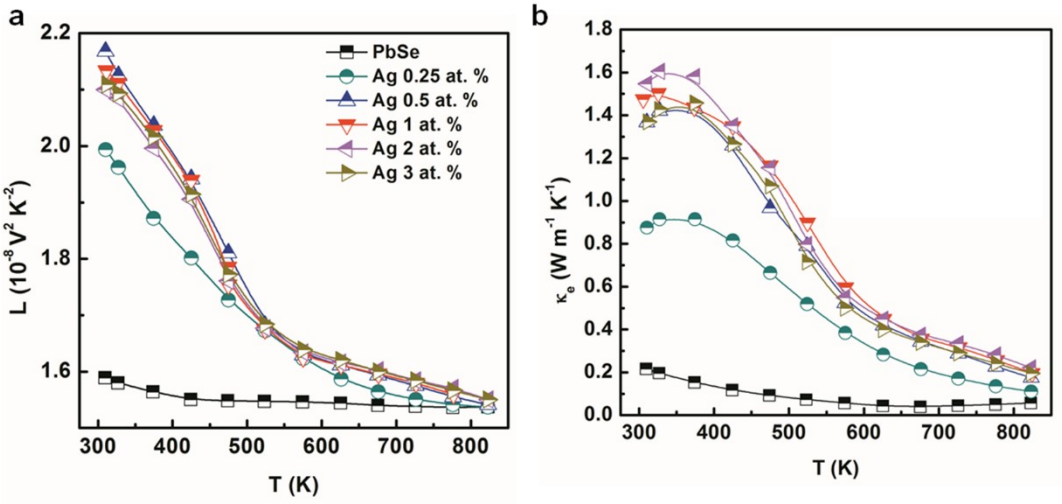

Fig. S2 Temperature dependent (a) the calculated Lorenz number based on single band model and electron-phonon interaction, (b) the electrical thermal conductivity (κ_e) calculated by Wiedemann-Franz law.

Section 3: Microstructure analysis of pore size distribution for Ag-doped PbSe

Multi-size pores have been found in all SHSed PbSe samples, as shown in Fig. S3.

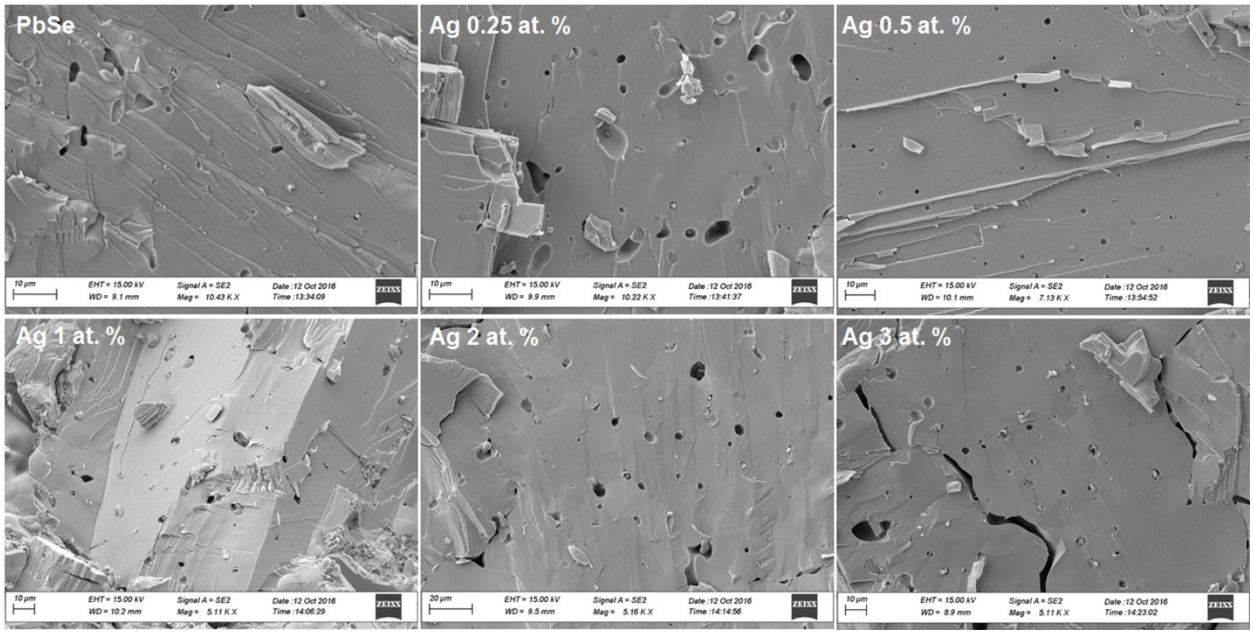

Fig. S3 Multi-size pores in SHSed $Pb_{1-x}Ag_xSe$ (x: 0-0.03).

To take a deep analysis of effects from pores, we count the numbers of them (over 500 per sample) and provide the distribution of size-dependent pore number at various doping level through SEM, the results are shown in Fig. S4a-b. Average pore sizes were achieved based on Gauss simulation, respectively 300 nm, 500 nm, 650 nm, 1.45 μm, 1.3 μm and 1.65 μm in $Pb_{1-x}Ag_xSe$ (x=0, 0.0025, 0.005, 0.01, 0.02, 0.03). Pore size keeps increasing until nominal Ag potent over 1 at. %, which demonstrates that Ag doping could effectively affect production of pores once it gets into the lattice of PbSe.

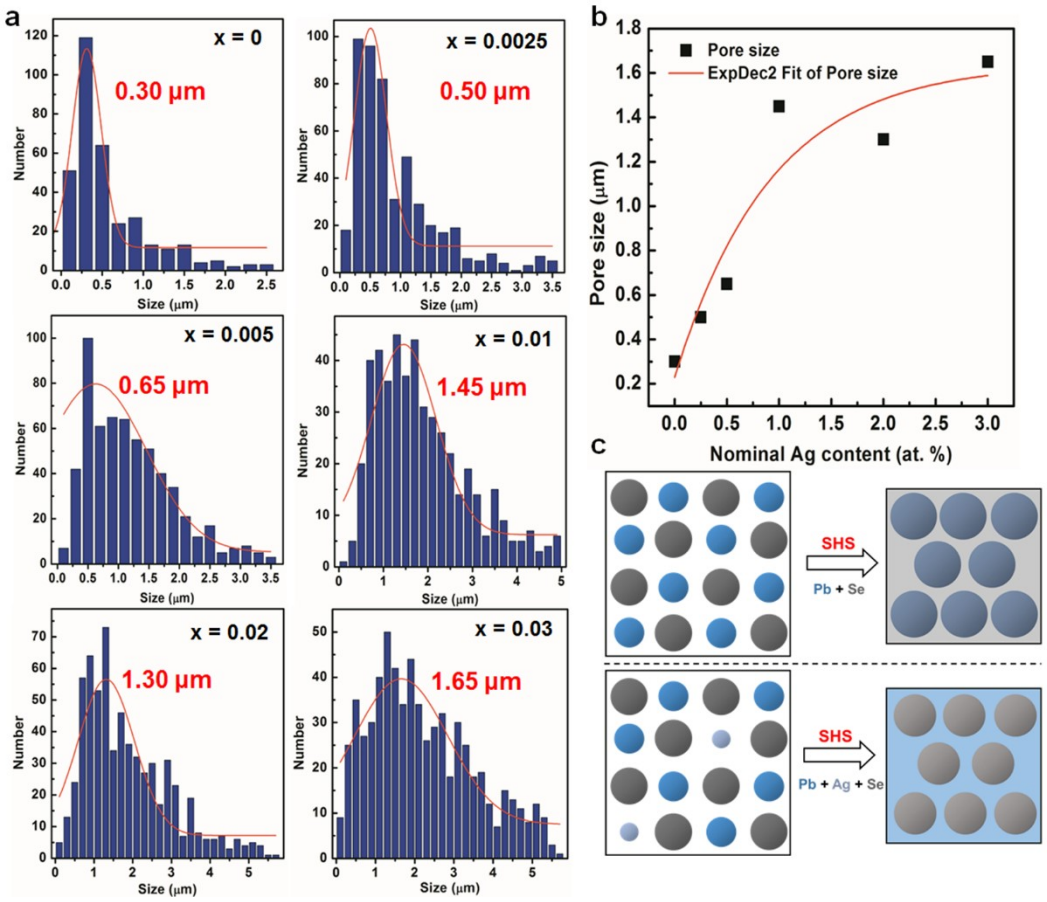

Fig. S4 Pore size variation of $Pb_{1-x}Ag_xSe$. (a) The Size distribution histograms of $Pb_{1-x}Ag_xSe$ (x=0, 0.0025, 0.005, 0.01, 0.02, 0.03). (b) Nominal Ag content – dependent pore size. (c) The anticipated effect of Ag doping for pore size.

Apart from high pressure and temperature provided by SPS sintering, all the pellets have to get through SHS process. One of numerous characteristics in this reaction is drastic heat release, and thermal expansion based on it would produce a lot of pores. Besides, liquid as well as pneumatolytic elements during SHS also play a big role in pore formation, as they will flow or move to other locations to take part in corresponding reactions. However, the reason for size distributions are still unclear, we suppose it could come from atom size difference of Ag and Pb. The size of Ag^+ (coordination number: n=6) is 1.15 Å, which is smaller than 1.19 Å of Pb^{2+} (n=6), therefore, though XRD cannot distinguish peak movement of $Pb_{1-x}Ag_xSe$ due to system error and low doping level (< 5 at. %), size difference of these two atoms possibly make great contribution in decreasing the size of $Pb_{1-x}Ag_xSe$ grains with more Ag doping, further enlarging gap as well as

pore size between $Pb_{1-x}Ag_xSe$ grains in mesoscopic scale, as shown in Fig. S4c.

Section 4: A comparison of thermoelectric properties for PbSe material system.

Table S1. A comparison of maximum *ZT* and average *ZT* for this work and some literature.

System	Constituent	Type	ZT_{max}	ZT_{avg}	*T*
PbSe	$Cu_{0.005}PbSe_{0.99}Te_{0.01}$[3]	n	1.7@773K	1.30	400-773K
	PbSe–18%SnS–0.5%Cu[4]		1.6@773K	1.13	300-873K
	$Pb_{0.997}Sb_{0.003}Se$[5]		1.5@830K	\	\
	$PbSe_{0.998}Br_{0.002}Se$-2%Cu_2Se[6]		1.8@723K	1.10	300-823K
	$Pb_{0.89}Sb_{0.012}Sn_{0.1}Se_{0.5}Te_{0.25}S_{0.25}$[7]		**1.8@900K**	**1.02**	**293-800K**
	$Pb_{0.8}Na_{0.1}Sb_{0.08}Cd_{0.02}Se$[8]	p	1.6@850K	0.95	300-850K
	$Pb_{0.98}K_{0.02}Se$-6%CdSe[9]		1.4@923K	0.83	400-923K
	$Pb_{0.99}Ag_{0.01}Se$-1.5%SrSe[10]		1.2@873K	0.86	400-923K
	$Pb_{0.95}Na_{0.02}Cd_{0.03}Se_{0.85}Te_{0.15}$[11]		1.7@900K	1.00	400-900K
	$Pb_{0.98}Na_{0.02}Se$-2%HgSe[12]		1.7@970K	\	\
	This work-$Pb_{0.99}Ag_{0.01}Se$		1.2@773K	1.10	523-823K

References

1. H. Wang, Y. Pei, A. D. LaLonde and G. J. Snyder, *Advanced Materials*, 2011, **23**, 1366-1370.
2. J. L. Lan, Y. C. Liu, B. Zhan, Y. H. Lin, B. Zhang, X. Yuan, W. Zhang, W. Xu and C. W. Nan, *Advanced Materials*, 2013, **25**, 5086-5090.
3. C. Zhou, Y. Yu, Y.-L. Lee, B. Ge, W. Lu, O. Cojocaru-Mirédin, J. Im, S.-P. Cho, M. Wuttig and Z. Shi, *Journal of the American Chemical Society*, 2020, **142**, 15172-15186.
4. Y. Xiao, L. Xu, T. Hong, H. Shi, S. Wang, X. Gao, X. Ding, J. Sun and L.-D. Zhao, *Energy & Environmental Science*, 2022.
5. Y. Lee, S.-H. Lo, C. Chen, H. Sun, D.-Y. Chung, T. C. Chasapis, C. Uher, V. P. Dravid and M. G. Kanatzidis, *Nature communications*, 2014, **5**, 1-11.
6. C. Zhou, Y. Yu, Y. K. Lee, O. Cojocaru-Mirédin, B. Yoo, S.-P. Cho, J. Im, M. Wuttig, T. Hyeon and I. Chung, *Journal of the American Chemical Society*, 2018, **140**, 15535-15545.
7. B. Jiang, Y. Yu, J. Cui, X. Liu, L. Xie, J. Liao, Q. Zhang, Y. Huang, S. Ning and B. Jia, *Science*, 2021, **371**, 830-834.
8. J. Cai, J. Yang, G. Liu, L. Xu, X. Wang, H. Hu, X. Tan and J. Jiang, *Advanced Energy*

Materials, 2022, 2103287.

9. S. Cai, S. Hao, Z.-Z. Luo, X. Li, I. Hadar, T. P. Bailey, X. Hu, C. Uher, Y.-Y. Hu and C. Wolverton, *Energy & Environmental Science*, 2020, **13**, 200-211.
10. Z. Z. Luo, S. Cai, S. Hao, T. P. Bailey, I. Spanopoulos, Y. Luo, J. Xu, C. Uher, C. Wolverton and V. P. Dravid, *Angewandte Chemie International Edition*, 2021, **60**, 268-273.
11. G. Tan, S. Hao, S. Cai, T. P. Bailey, Z. Luo, I. Hadar, C. Uher, V. P. Dravid, C. Wolverton and M. G. Kanatzidis, *Journal of the American Chemical Society*, 2019, **141**, 4480-4486.
12. J. M. Hodges, S. Hao, J. A. Grovogui, X. Zhang, T. P. Bailey, X. Li, Z. Gan, Y.-Y. Hu, C. Uher and V. P. Dravid, *Journal of the American Chemical Society*, 2018, **140**, 18115-18123.